# Co-deposition of silica and proteins at the interface between two immiscible electrolyte solutions

Poltorak, Lukasz; van der Meijden, Nienke; Skrzypek, Sławomira; Sudhölter, Ernst J.R.; de Puit, Marcel

**DOI**
10.1016/j.bioelechem.2020.107529

**Publication date**
2020

**Document Version**
Final published version

**Published in**
Bioelectrochemistry

Bioelectrochemistry 134 (2020) 107529

Contents lists available at ScienceDirect

Bioelectrochemistry

journal homepage: www.elsevier.com/locate/bioelechem

# Co-deposition of silica and proteins at the interface between two immiscible electrolyte solutions

Lukasz Poltorak [a,b,*], Nienke van der Meijden [b], Sławomira Skrzypek [a], Ernst J.R. Sudhölter [b], Marcel de Puit [b,c]

[a] Department of Inorganic and Analytical Chemistry, Faculty of Chemistry, University of Lodz, Tamka 12, 91-403 Lodz, Poland
[b] Delft University of Technology, Department of Chemical Engineering, Van der Maasweg 9, 2629 HZ Delft, the Netherlands
[c] Netherlands Forensic Institute, Forensic Biometric Traces, Laan van Ypenburg 6, 2497 GB The Hague, the Netherlands

ARTICLE INFO

*Article history:*
Received 19 February 2020
Received in revised form 2 April 2020
Accepted 2 April 2020
Available online 8 April 2020

*Keywords:*
Electrified liquid-liquid interface
The sol-gel process of silica
Interfacial deposition
Haemoglobin
Acid phosphatase
α-amylase

ABSTRACT

In this work, we have simultaneously examined, electrochemically driven deposition of three proteins (haemoglobin, acid phosphatase, and α-amylase) and silica films at a polarized liquid–liquid interface. The interfacial adsorption of the proteins occurs efficiently within the acidic pH range (pH = 2–4). The interfacial charge transfer reactions recorded in the presence of fully positivity charged macromolecules were followed with cyclic voltammetry on the positive side of the potential window. Faradaic currents attributed to the presence of proteins in the aqueous phase appeared for concentrations equal to ca. 0.1 μM for haemoglobin and acid phosphatase and ca. 1 μM for the α-amylase. Concomitant deposition of silica films was achieved via the addition of tetraethoxysilane molecules to the organic phase (1,2-dichloroethane). The hydrolysis and condensation reactions of tetraethoxysilane were controlled *via* the interfacial transfer of $H^+$ coinciding with the potential for protein adsorption. The effect of tetraethoxysilane concentration – up to 50% by volume – revealed significant shrinkage of the potential window (the region where capacitive currents are recorded). The optimized platform was then used to prepare silica-proteins co-deposits. These could be easily collected from the interface and further analyzed with infrared spectroscopy and transmission electron microscopy.



## 1. Introduction

Interaction, immobilization or attachment of bio-components with or to inorganic materials provide a platform that merges the properties of both systems. Bio-molecules such as enzymes, antibodies, DNA, cellular building blocks (among many other examples) carry in unique properties that find applications in sensing [1,2], biomimetic interfaces construction [3–5], bio-catalysis [6,7] or bio-energetics [8,9]. In turn, the wide range of inorganic materials provides complementary benefits, like their inert supporting properties, electric conductivity, mesoporosity or susceptibility towards additional post-grafting procedures. Further liaison with the electrochemical input (e.g. system perturbation, interface modification) or output (e.g. electroanalytical data collection) in a form of solid electrodes or soft junctions extends their applicability and also our understanding of such platforms.

Electrified liquid–liquid interface (LLI) – or the interface between two immiscible electrolyte solutions (ITIES) [10,11] – is an electrochemical platform where the interfacial transfer of charged species give rise to currents that can be probed with all methods offered by an electrochemical toolbox. Few interfacial charge transfer reaction mechanisms were revealed to date [12] with simple ion transfer, facilitated ion transfer and electron transfer reactions being in the core. Interestingly, charged or ionizable macromolecules undergo similar interfacial charge transfer reaction mechanisms. Successive polarization of the interfacial region leads to the adsorption of macromolecules to the LLI. Further polarization, together with the accumulated positive or negative charge within defined locus, facilitates the transfer of the organic phase background electrolyte anions or cations, respectively. This type of interfacial behaviour was reported for dendrimers (poly-L-lysine [13]; poly(propylamine) [14]; poly(amidoamine) [14,15] or carboxyl terminated-poly(amidoamine) [16]), polyelectrolytes (poly(diallyl dimethylammonium chloride) [17]; chitosan [18] protamine [19]; heparin [20]), proteins (e.g. ferritin [21] haemoglobin (Hb) [22,23]; myoglobin [24]; insulin [25]; cytochrome [26]) or DNA (thrombin binding aptamer [27]). Resulting deposits usually reside at the interface in a form of thin films.

* Corresponding author at: Department of Inorganic and Analytical Chemistry, Faculty of Chemistry, University of Lodz, Tamka 12, 91-403 Lodz, Poland.
*E-mail address:* lukasz.poltorak@chemia.uni.lodz.pl (L. Poltorak).

https://doi.org/10.1016/j.bioelechem.2020.107529
1567-5394/

The Janus properties (intrinsic asymmetry defined by two immiscible solvents) of the polarized LLI allow for the separation of reagents whose interfacial reaction may result in interfacial deposit formation. An example could be the electron transfer reaction between the metal ion complex initially present in the water phase and the electron donor (usually derivatized ferrocene species) dissolved in the organic phase. Supply of the energy in the form of an applied potential difference allows for the e.g. Pt [28,29], Pd [28–30] or Au [31] nanoparticles formation within the interfacial region. Different interfacial modification strategies can be based on the electrochemically controlled ion transfer reaction followed by the interfacial precipitation. Surfactant templated mesoporous silica materials were generated by using this approach. Briefly, the cationic surfactant template initially present in the organic phase is transferred to the water phase containing silanol species. The formation of positively charged micelles catalyzes the silica condensation process with the subsequent silica gel layer residing at the LLI [32–36]. As the silica sol-gel processing is highly dependent on the aqueous phase pH, both the hydrolysis and condensation reaction can be controlled *via* interfacial $H^+$ transfer [32,37] or pH gradients created at the three-phase junction [38]. These are examples allowing for the precise control of the deposit location, this is at the boundary between at least two phases having distinct physicochemical properties.

In this work, we extend our previous study, [37] showing the possibility of acid phosphatase (AP) immobilization within the silica matrix at the polarized LLI. Our approach combines the possibility of electrochemically controlled interfacial adsorption of proteins (the AP, the Hb, and the α-amylase) and electrodeposition of the silica film. This is possible since the protein adsorption process and the interfacial transfer of $H^+$ to the organic phase, where it catalyzes tetraethoxysilane (TEOS – silica precursor) hydrolysis and condensation reactions, occur at similar positive potential values. The co-deposition process was optimized in terms of TEOS loading in the organic phase, protein concentration and the pH of the aqueous phase. Formed interfacial deposits were visible with the naked eye and could be collected from the interface for further analysis. This work opens new avenues allowing for biocomponents immobilization at soft junctions, were the inorganic material help prevent the direct contact between e.g. sensitive proteins and organic solvents.

## 2. Methods and materials

### 2.1. Materials

Sodium chloride (NaCl, >99%, Sigma-Aldrich), citric acid monohydrate ($C_6H_8O_7$, ≥99%, Sigma-Aldrich) served as the aqueous phase background electrolytes. Acid phosphatase (AP) from wheat germ, haemoglobin (Hb) from bovine blood and α-amylase from *Aspergillus oryzae* – all from Sigma-Aldrich - were selected as model proteins. Tetraethoxysilane (TEOS, 98%, Sigma-Aldrich) was used as the silica precursor. 1 M HCl or 1 M NaOH from Merck were used to adjust the pH of the aqueous phase. The organic phase background electrolyte (bis(triphenylphosphoranylidene)ammonium tetrakis(4-chlorophenyl)borate – BTPPATPBCl) was precipitated by mixing equimolar amounts of bis(triphenylphosphoranylidene)ammonium chloride (BTPPACl, 97%, Sigma-Aldrich) and potassium tetrakis(4-chlorophenyl)borate (KTPBCl, 98%, Sigma-Aldrich). For details see [39].

### 2.2. Electrochemical set-up

All electrochemical experiments performed in this study were supported by the Autolab PGSTAT302N. Two types of electrochemical glass cells were employed to support both immiscible liquids: (i) one having two Luggin capillaries with the LLI placed in between (cell radius = 0.65 cm) [40] and the second cell with one capillary fixed to the cell bottom and second removable capillary that was introduced from the top (cell radius = 1.00 cm). The interfacial polarization was performed through a four-electrode configuration with two Ag/AgCl reference electrodes placed in the cell's capillaries and two Pt counter electrodes, one of each type placed in the aqueous and the organic phase. Currents recorded during all electrochemical experiments do not originate from the oxidation/reduction reactions (the system is deprived of the classical working electrode) and are the consequence of the ions crossing the LLI. Corresponding electrochemical cells apply for this work:

$$Ag|AgCl|\begin{matrix}10\ mM\\ HCl\end{matrix}\Big|\Big|\begin{matrix}x\%\ vol\ TEOS\\ 10\ mM\ BTPPATPBCl\end{matrix}\Big|\begin{matrix}10\ mM\ NaCl\\ 10\ mM\ BTPPACl\end{matrix}|AgCl|Ag \quad \text{(cell I)}$$

$$Ag|AgCl|\begin{matrix}10\ mM\ HCl\\ y\ \mu M\ protein\end{matrix}\Big|\Big|\begin{matrix}10\ mM\\ BTPPATPBCl\end{matrix}\Big|\begin{matrix}10\ mM\ NaCl\\ 10\ mM\ BTPPACl\end{matrix}|AgCl|Ag \quad \text{(cell II)}$$

$$Ag|AgCl|\begin{matrix}citric\ acid\ buffer(pH=z)\\ 10\ mM\ NaCl\\ w\ \mu M\ protein\end{matrix}\Big|\Big|\begin{matrix}30\%\ vol\ TEOS\\ 10\ mM\ BTPPATPBCl\end{matrix}\Big|\begin{matrix}10\ mM\ NaCl\\ 10\ mM\ BTPPACl\end{matrix}|AgCl|Ag \quad \text{(cell III)}$$

### 2.3. Infra-red spectroscopy

Infra-red spectra were recorded with a Nicolet 8700 FT-IR spectrometer. Around 2–3 mg of dried silica-based films collected from the interface were mixed with the KBr powder giving around 100 mg of the final mixture. Next, KBr pellet was prepared and the transmission spectra were collected from 4000 $cm^{-1}$ to 500 $cm^{-1}$ (resolution = 4 $cm^{-1}$).

### 2.4. Transmission electron microscopy

Nanomorphology of silica films collected from the LLI was investigated with the Transmission Electron Microscopy technique using JEOL JEM-1400 Plus (the USA) at operating voltage equal to 200 kV. The suspension of silica powder in EtOH was drop cast onto the copper mesh support. After drying the mesh in desiccator the TEM investigation was performed.

## 3. Results and discussion

### 3.1. Electrochemically controlled silica deposition

The electrochemically controlled interfacial deposition of silica was performed in a configuration where silica precursors (TEOS) is initially dissolved in the organic phase (1,2-dichloroethane) whereas adjacent water phase is acidified, and hence, provides protons having the ability to catalyze TEOS hydrolysis and subsequent condensation reactions. This protocol is an alternative to a few other methods allowing for silica formation at the interfacial region. These include (i) surfactant templated interfacial silica deposition arising from the electrochemically controlled reaction between silanol species and cationic template initially present in the water (pH ~ 9) and the organic phase respectively [32–36] or (ii) *ex situ* interfacial modification relying on externally prepared silica membranes that are further used to support the ITIES [41–44]. The schematic representation of series of reactions occurring at the LLI during silica deposition studied in this work is depicted in Fig. 1A. The standard Galvani potential of the $H^+_{aq\rightarrow org}$

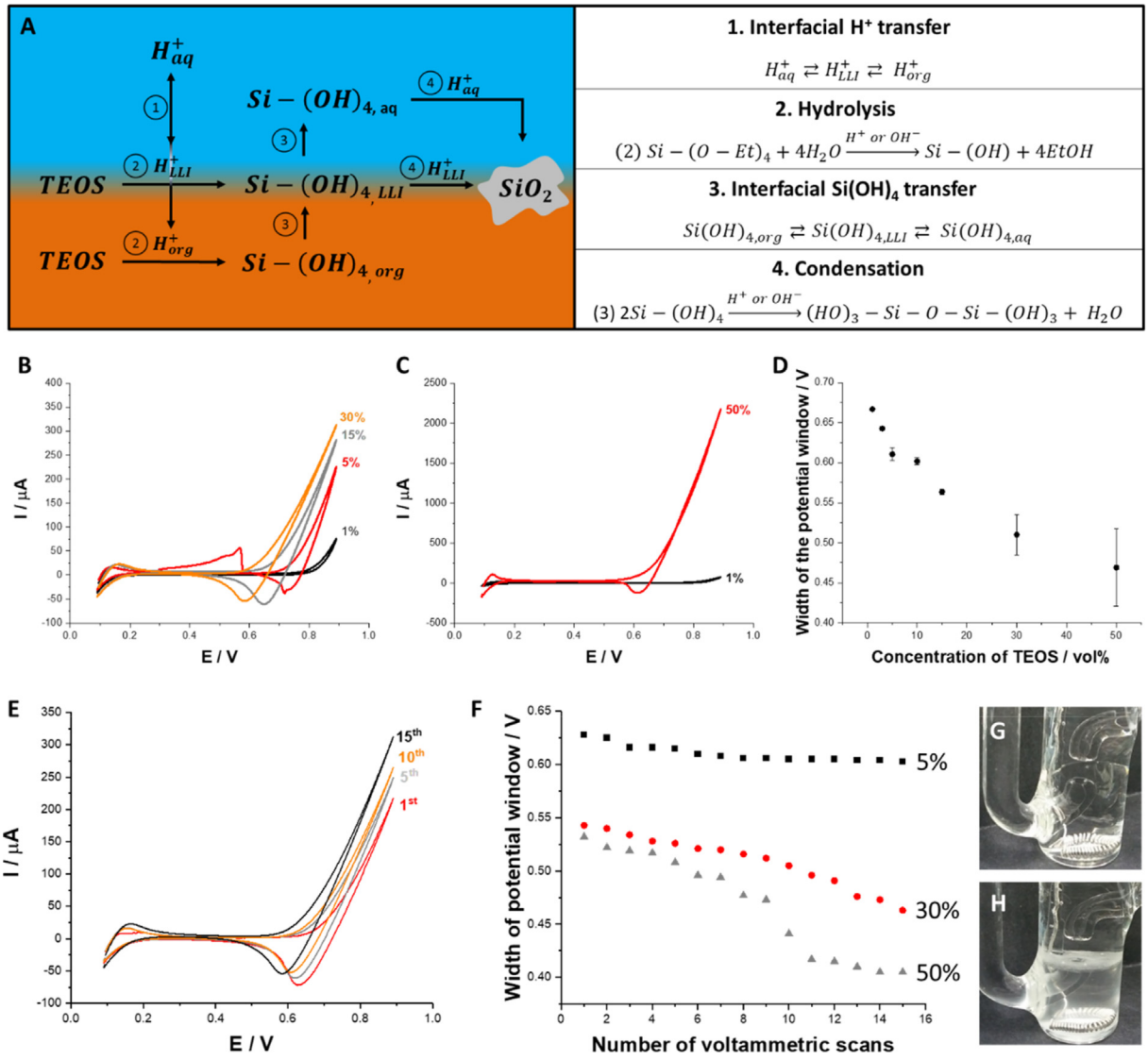


**Fig. 1.** A shows the schematic representation of a few mutually connected reactions occurring at the polarized LLI during the proposed silica deposition reaction. B and C are cyclic voltammograms (CVs) recorded for different vol% TEOS in the organic phase as indicated on the right of each curve. D – is the width of the potential window averaged over 15 scans for different vol% TEOS. E – shows consecutive CVs recorded for vol% TEOS in the organic phase equal to 30%, the number of cycles is indicated on the right of each curve. F – is the width of the potential window for three different vol% TEOS in the organic phase as indicated on the right of the graph. G and H are the photos recorded before and after 15 voltammetric cycles (vol% TEOS = 50%), respectively. For all CVs the scan rate was 10 $mV \cdot s^{-1}$. The aqueous phase was 10 mM HCl.

equals to 0.55 V [40] and is lower than 0.59 V found for $Na^+_{aq\rightarrow org}$ and $Li^+_{aq\rightarrow org}$ usually limiting the potential window (defined as the region of the voltammogram where, in the presence of only background electrolyte ions, capacitive currents are recorded) on the positive side of the voltammograms. This means that voltammograms recorded in Cell I with only 10 mM HCl used as the aqueous phase background electrolyte

will be limited by the $H^+_{aq\rightleftarrows org}$ on a more positive potential side and $Cl^-_{aq\rightleftarrows org}$ on the less positive potential side. With the forward polarization towards more positive potential values protons from the aqueous phase will eventually reach the LLI and further transfer to the organic phase (Fig. 1A – reaction (1)). The increasing concentration of protons within the interfacial region catalyzes the hydrolysis of TEOS which gives silanol species and EtOH as the hydrolysis product (Fig. 1A – reaction (2)). Since silanols are more hydrophilic than ethoxy silanes (e.g. theoretical predictions of $LogP_{water/octanol}$ equals to 5.10 and 0.65 for TEOS and orthosilicic acid respectively [45]) their partitioning from the organic phase to the LLI and further to the aqueous phase will occur (Fig. 1A – reaction (3)). Protons from the water phase or available in the mixed layer region of the LLI will now catalyze the subsequent condensation of silanols to silica according to Reaction (4) from Fig. 1A. Finally, the formed silica is found as a deposit at the soft junction.

Fig. 1B and 1C show the effect of different concentrations of TEOS added to the organic phase on the shape of the recorded cyclic voltammograms (CVs). After adding 1% vol of TEOS to the organic phase the shape of the voltammogram barely changed over 15 consecutive scans as compared with blank (not shown). Further increase of the TEOS concentration causes a visible increase in the potential window limiting current on the positive potential side from 77 μA for blank and 1% vol TEOS to 284 μA for 15% vol TEOS and further to 2.2 mM for 50% vol TEOS. The positive current on the right-hand side of the voltammogram may be attributed to the interfacial ion transfer of protonated, and hence, positively charged silicic acid (pKa = 9.9) [46] or other silanol species from the aqueous to the organic phase. The change in interfacial polarization on

the reversed scan (from higher to lower potential values) draws the negative peak current which is due to reversed ion transfer reaction - protonated silicic acid back transfer from the organic to the aqueous phase. Also, as shown in Fig. 1D, we have noticed that the available potential window shrinks gradually from 0.67 V to 0.47 V with the increasing concentration of TEOS in the organic phase. This happens as the $H^+$ catalyzed hydrolysis reaction provides (i) interfacially active silicic acid species having a standard ion transfer potential lower than that reported for protons and (ii) EtOH which affects the structure of the LLI mixed layer region, or in other words, increases the mutual miscibility between water and 1,2-dichloroethane. The final factor affecting the voltammetric readout was the number of repetitions recorded in a single experiment as shown in Fig. 1E for 30% vol TEOS, or presented in Fig. 1F as the width of the potential window for three different TEOS concentrations. Again we have noticed shrinkage of the potential window and increasing limiting currents at more positive potential values with an increasing number of voltammetric cycles. This effect was especially prominent for higher concentrations of TEOS. Over 15 cycles the potential window was reduced by 4%, 15% and 24% for TEOS concentrations of 5, 30 and 50%, vol respectively. This indicates that the hydrolysis and condensation reactions are directly catalyzed by the electrochemical proton transfer from the water to the organic phase. Additionally, after a few voltammetric cycles, even for low concentrations of TEOS, white deposits appeared at the ITIES – see Fig. 1G (before deposition) and Fig. 1H (after 15 cycles for 50% vol TEOS). These deposits were then collected and analyzed with infra-red spectroscopy with the results shown in Fig. 2. The appearance of three characteristic absorption bands at 460 $cm^{-1}$ (Si—O bending), 802 $cm^{-1}$ (Si stretching) and 1086 $cm^{-1}$ (Si—O stretching) confirm that the electrochemically formed deposit is silica [47]. The peak at around 950 $cm^{-1}$ and the wide arm with a center around 1200 $cm^{-1}$ suggests the presence of non-hydrolyzed alkoxysilane functions (—Si—O—$CH_2$—$CH_3$) [48]. Other peaks are summarized in the caption of Fig. 2. To confirm that the silica deposition is controlled by electrochemistry we set the control experiment, this is 50% vol TEOS in the organic phase and 10 mM HCl in the aqueous phase with no external polarization, for which no deposit formation was observed up to 2 h. Just for comparison, for high concentrations of TEOS, the silica film was observed already after one voltammetric cycle (around 1 min).

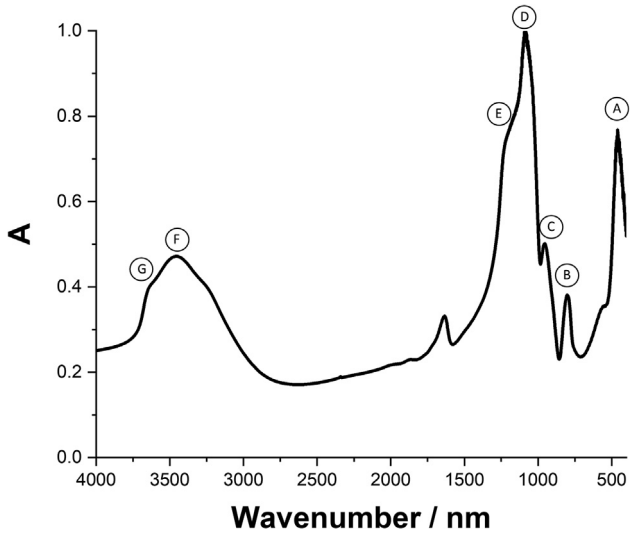


**Fig. 2.** Infra-red spectra of silica film collected from the interface after 15 consecutive cycles. pH of the aqueous phase was equal to 2. TEOS concentration in the organic phase was 50% vol. Absorption bands marked with letters correspond to: A – Si-O bending (460 $cm^{-1}$); B – Si stretching (802 $cm^{-1}$); C – Si—O—$CH_2$—$CH_3$ (958 $cm^{-1}$); D – Si—O stretching (1086 $cm^{-1}$); E – Si—O—$CH_2$—$CH_3$ (1202 (arm) $cm^{-1}$); F – Si—OH (3467 $cm^{-1}$); G – Free OH (3640 $cm^{-1}$).

### 3.2. Interfacial behavior of proteins

In this work, we have chosen three model proteins – the AP, the Hb) and α-amylase – that were studied at the ITIES. All molecules, build from the amino acid building blocks have to be charged in order to become interfacially active. Correspondingly, we have chosen 10 mM HCl (pH = 2) assuring the positive charge within the protein chain. Fig. 3A shows the blank voltammogram recorded in cell II for [protein] = 0 μM. Only the potential region where the Faradaic signals originating from the presence of positively charged macromolecules are expected to occur is shown. The current limiting the potential window at the more positive potential side is due to $H^+_{aq \rightleftarrows org}$.

Fig. 3B–D represent the voltammetric responses recorded in cell II (2)for [AP] = 10 μM; [Hb] = 12 μM and [α-amylase] = 16 μM respectively. The ion transfer voltammograms for AP and Hb share similar characteristics: (i) the intensities of the forward (positive) and reversed (negative) peak currents deviate from unity; (ii) current patterns hold irregular shapes – dissimilar to signals expected for reversible ion transfer reactions; (iii) the signals appear within the positive side of the potential window and (iv) the reversed peaks are terminated with the abrupt drop in a peak current indicating interfacial adsorption process. This is a very typical behavior of macromolecules at the electrified LLI indicating proteins interfacial adsorption process facilitating the transfer of the organic phase background anion (TPBCl in case of this study) [22,23,49,50]. The scan rate dependence (see Fig. S2 from supplementary information) performed for all proteins revealed the linear relationship of the positive peak current versus the square root from the scan rate meaning that the transfer of the interfacially active species towards the interface is governed by diffusion. All this indicates that the mechanism of the charge transfer reactions recorded in

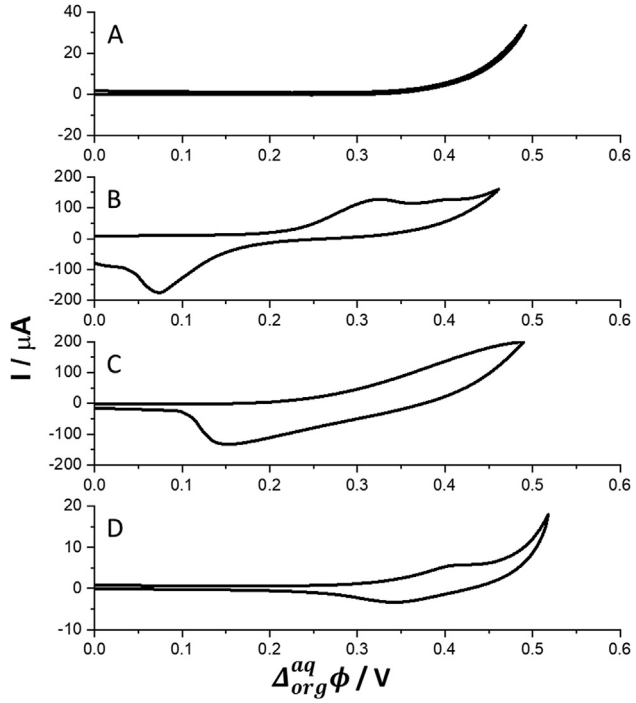


**Fig. 3.** A – Blank CV recorded in cell II. B – CV recorded for [Hb] = 10 μM; C – CV recorded for [AP] = 12 μM and D – CV recorded for [α-Amylase] = 16 μM. pH of the aqueous phase was equal to 2.

the presence of ionized proteins is governed by both diffusion and adsorption processes. At this point, we have to mention that these observations are in line with other reports [49–52]. Investigation of α-amylase appeared to be troublesome as this protein did not dissolve in the aqueous phase. Nevertheless, the blurry solution of α-amylase was subjected to electrochemical investigation still giving a Faradaic response – see Fig. 3D, S1 and S2-E (further discussion is available in supporting information).

The different behavior of Hb together with AP and the α-amylase can be also inferred from the calibration curves plotted in Fig. 4A. In the calibration patterns recorded for the Hb and the AP three linear ranges can be noticed. (i) The first one, having a relatively low slope, for protein concentrations up to around 1 μM that can be attributed to the formation of a protein monolayer. (ii) The region with the highest sensitivity from 1 μM to around 6 μM which we think is due to the protein multilayer build-up. As the facilitated transfer of the organic phase background electrolyte anion from the organic phase to the interfacial region is directly proportional to the surface charge, this is the region experiencing the highest charge increments per voltammetric cycle. (iii) Eventually, the positive peak currents reach a plateau (for the Hb) or gradually lose sensitivity (for AP). At this point, we can speculate that the thickness of the protein film is self-screening the positive charge from the outer layers. Correspondingly, the signal intensity decreases or simply saturates. The table in Fig. 4B summarizes the fitting parameters of the linear regression line fitted to the region showing the highest sensitivity. Obtain slopes can be qualitatively attributed to the charge increments accumulated at the LLI being highest for the Hb (slope = 35.67 $A{\cdot}M^{-1}$) followed by slightly lower value for the AP (slope = 18.21 $A{\cdot}M^{-1}$) to finally mention the α-amylase giving two orders of magnitude lower value (Fig. S1-A, slope = 0.13 $A{\cdot}M^{-1}$). After performing the calibration experiment the photos of the LLI were taken and are shown in Fig. 4C (the non-modified LLI depicted for comparison) and Fig. 4D–F. Clear and visible with naked eye films were present at the interface for the Hb (dark and uniform layer, Fig. 4D) and AB (wrinkled deposit, Fig. 4E) only after voltammetric cycling further confirming electrochemically controlled adsorption process. Since the adsorption process for all three studied portions can be controlled electrochemically only for the HB and the AP, the α-amylase was excluded from the co-deposition protocol described in the following section.

### 3.3. Concurrent deposition of proteins and silica

The electrochemical co-deposition of silica and protein was performed in cell III. During all experiments, we have set the concertation of the Hb and the AP in the aqueous phase to 4 μM. The concentration of TEOS in the organic phase was chosen to be 30% vol which is a compromise between the formation of a compact and removable (from the interface) silica film and the width of the potential window. Fig. 5A and 5B show the CVs recorded at three different pH values for Hb and AP, respectively. The CVs for the Hb and the AP recorded at pH = 2.8 share similar characteristics. Signals originating from the proteins are overlaid with the limiting current on the more positive potential side – the interfacial transfer of the protonated silicic acid. The Hb gave a clear forward and reversed peak at pH = 3.9 and 4.9 indicating that it is a protein rather than hydrolyzed TEOS species which contributes to the recorded signal. Although each voltammogram exhibits distinct shape, we did not find a correlation that could explain the shared behavior of the Hb and the AP in the presence of TEOS in the organic phase. We can, however, conclude that the charge transfer reaction triggered in the presence of charged macromolecules in the water phase and TEOS in the organic phase can still be followed using voltammetry.

To choose the appropriate pH for the proteins and silica co-deposition, we further investigated the change in the capacitive current over 50 consecutive voltammetric cycles. Results for three different pH values are shown in Fig. 6A (for the Hb) and Fig. 6B (for the AP). Since the capacitive current for the first cycle was dependent on the pH we normalized the data set by dividing all points from a series by the value of the first point. In this way, we can follow the change in the surface charge as we repeatedly polarize the ITIES. Although this effect is slightly more pronounced for the Hb, the separation between the capacitive currents grows only for the lowest studied pH of 2.8. Two other pH values displayed rather a stationary tendency. We have attributed the

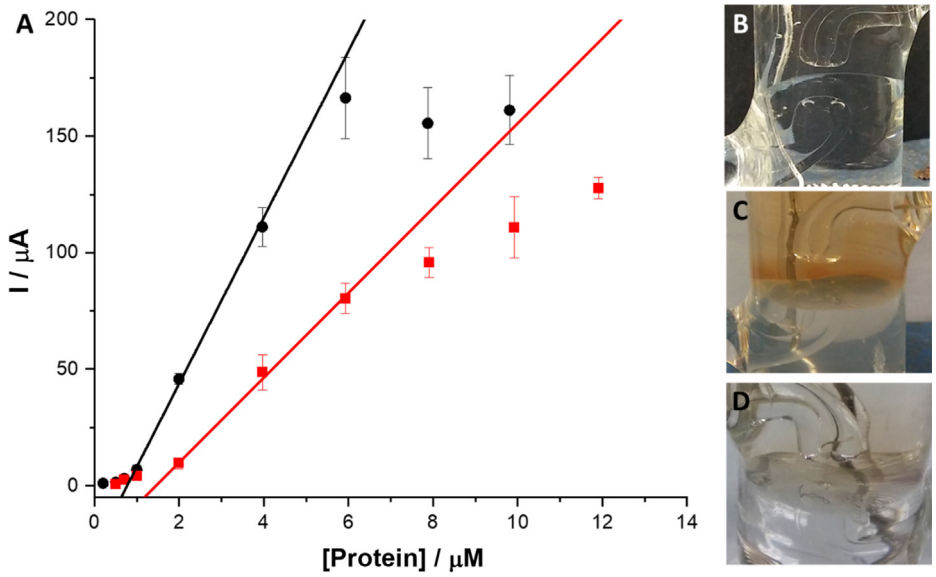


**Fig. 4.** A – Positive peak current in function of Hb (black circles) and AP (red squares) concentration. Linear fit equation for the Hb is y = 35.67x ($A{\cdot}M^{-1}$) – 2.75 (μA); $R^2$ = 0.989 (n = 4) and for the AP is y = 18.21x ($A{\cdot}M^{-1}$) – 2.65; $R^2$ = 0.997 (n = 3). Photos of the LLI: B – before interfacial modification; C – after Hb deposition; D – after AP deposition. The data points in the calibration curves were collected using cyclic voltammetry (scan rate = 10 $mV{\cdot}s^{-1}$).

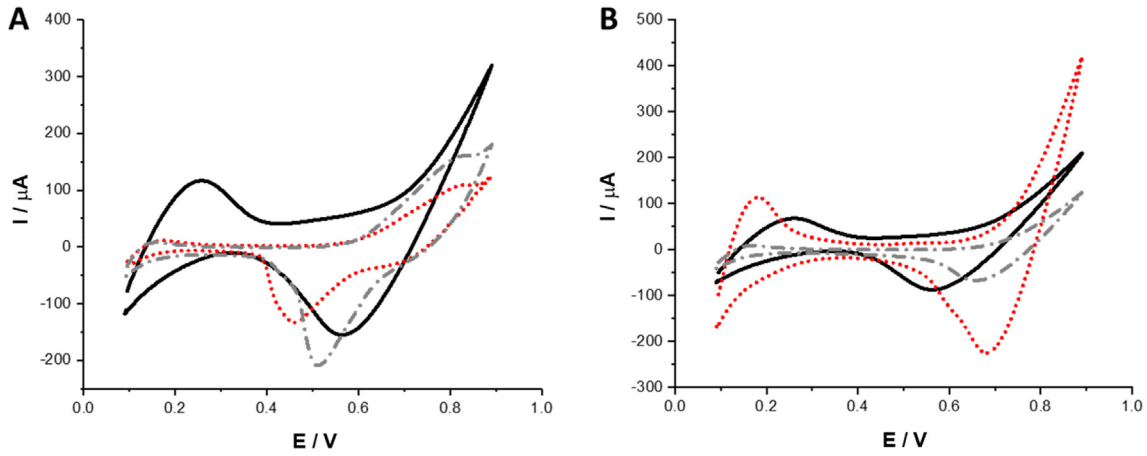


**Fig. 5.** 50th CV scan from the repetition series recorded for the Hb (A) and the AP (B) at three different pH values as indicated in the legend. The vol% of TEOS in the organic phase equals to 30% in all cases; [Hb] and [AP] were set to 4 μM. CVs recorded in Cell III for z = 2.8 (black solid line), 3.9 (red dotted line) or 4.9 (grey dash-dot line).

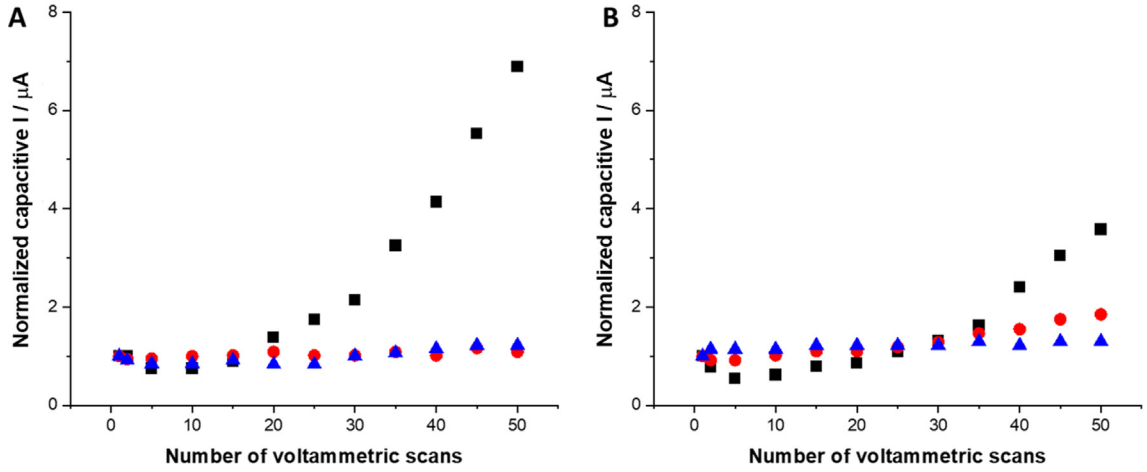


**Fig. 6.** Capacitive current in the function of a number of CV cycles recorded for 4 μM Hb (A) or AP (B). The vol% of TEOS in the organic phase equals 30% in all cases; pH of the aqueous phase is 2.8 (black squares); 3.9 (red circles) and 4.9 (blue triangles). The capacitive current was measured at E = 0.4 V.

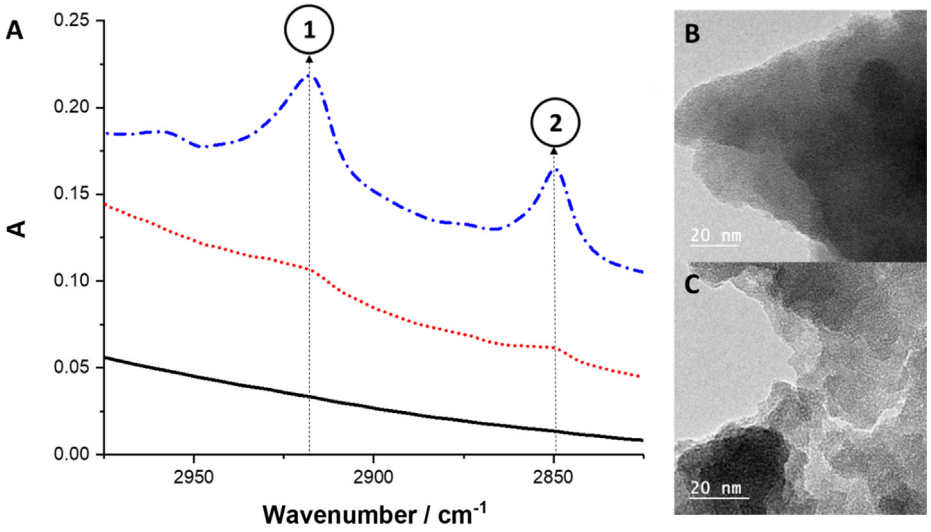


**Fig. 7.** A – Infra-red spectra recorded for blank $SiO_2$ (black solid line), the AP co-deposited with $SiO_2$ (red dotted line) and the Hb co-deposited with $SiO_2$ (blue dash-dotted line) Numbers (1) and (2) correspond to absorption bands centers equal to 2918 $cm^{-1}$ and 2849 $cm^{-1}$ respectively. B and C are the TEM micrographics recorded for the Hb co-deposited with silica films.

change in the capacitive current separation to successive positive charge accumulation in a form of electrodeposited silica (pKa = 4.0–4.3) [53], silica terminated with protonated silanol groups and positively charged proteins. Consequently, we have chosen the pH = 2.8 as the optimal for the proteins and silica co-deposition.

Finally, we used the electrochemical cell with the largest surface area to generate sufficient amount of material for further characterization. In this respect, we used infra-red spectroscopy with the region of interests shown in Fig. 7A. Three samples were analyzed (i) silica deposited at the LLI in the absence of proteins; (ii) silica deposited at the LLI in the presence of the AP and (iii) silica deposited at the LLI in the presence of the Hb. The deposit formation protocol was the same in all three cases. The potential equal to 0.9 V was applied for 30 min giving a thick layer of proteins and silica that was subsequently collected and dried. Since silica absorbs strongly in the infra-red range from 400 $cm^{-1}$ to 1500 $cm^{-1}$ only the region from around 2800 $cm^{-1}$ to 3000 $cm^{-1}$ was analyzed to confirm the presence of proteins. These appeared as two absorption bands with the peaks located at 2849 $cm^{-1}$ and 2918 $cm^{-1}$ which can be attributed to the $CH_2$ antisymmetric and $CH_2$ and $CH_3$ symmetric stretching modes [54]. Also, we have studied the Hb and silica co-deposited material with the transmission electron microscope and the results are depicted in Fig. B and C. Obtained micrographics indicate that the resulting material exhibits porosity defined by elongated pores. Its morphology is similar to silica templated by cationic surfactant at the electrified LLI [33].

In the future, we want to apply our methodology to support enzymes at the ITIES. Carefully chosen enzymes (the focus will be given to enzymes for which optimal working conditions fall for the acidic pH, e.g. AP), reaction substrates and products having different partitioning properties, may give an elegant platform where the bio-component will be separated from the denaturing organic phase by the inorganic material. In turn, separation of the reactants and products of the enzymatic reaction will be achieved by the soft junction. Since the synthetic conditions applied in this work (silica-protein deposition requires low pH of the aqueous phase) may lead to protein denaturation, *ex-situ* prepared protein-inorganic deposits will be also investigated.

## 4. Conclusions

In this work, we have described and discussed three mutually interconnected subjects. (i) The comprehensive study of the silica film formation at the liquid-liquid interface that is catalyzed by the electrochemically controlled proton transfer from the water to the organic phase containing TEOS (silica precursor). We found that TEOS added to the organic phase at the elevated concentrations (up to 50% vol) significantly reduces the available potential window and gives intense limiting positive currents that were attributed to protonated silanol species crossing the interface. Also, repetitive voltammetric cycling resulted in the silica film deposition. (ii) The electrochemical behavior of three model proteins (the AP, the Hb, and the α-amylase) at the electrified liquid-liquid interface. As reported by others and confirmed in this study, the AP and the Hb were electrochemically active and were adsorbed to the liquid-liquid interface forming films that were visible with the naked eye. Although the α-amylase was insoluble in the acidified water phase we were still able to record Faradaic signals originating from its charged flakes residing at the ITIES. Finally, (iii) electrochemically controlled co-deposition of proteins and the silica film at the ITIES was investigated. We succeeded in placing both bio- and inorganic components within the defined locus. Afterward, the films were collected and analyzed using infra-red spectroscopy (confirming the presence of proteins) and transmission electron microscopy (revealing the silica surface morphology) imaging.

## Declaration of Competing Interest

The authors declare that they have no known competing financial interests or personal relationships that could have appeared to influence the work reported in this paper.

## Acknowledgments

The authors are grateful to Wiel Evers for performing TEM analysis. Lukasz Poltorak is grateful for the financial support from the National Science Center (NCN) in Krakow, Poland (Grant no. UMO-2018/31/D/ST4/03259).

## Appendix A. Supplementary material

Supplementary data to this article can be found online at https://doi.org/10.1016/j.bioelechem.2020.107529.

## References

[1] R.K. Shervedani, A.H. Mehrjardi, N. Zamiri, A novel method for glucose determination based on electrochemical impedance spectroscopy using glucose oxidase self-assembled biosensor, Bioelectrochemistry 69 (2006) 201–208, https://doi.org/10.1016/j.bioelechem.2006.01.003.
[2] B. Jiang, M. Wang, Y. Chen, J. Xie, Y. Xiang, Highly sensitive electrochemical detection of cocaine on graphene/AuNP modified electrode via catalytic redox-recycling amplification, Biosens. Bioelectron. 32 (2012) 305–308, https://doi.org/10.1016/j.bios.2011.12.010.
[3] M. Kruszewski, M. Kusaczuk, J. Kotyńska, M. Gál, R. Krętowski, M. Cechowska-Pasko, M. Naumowicz, The effect of quercetin on the electrical properties of model lipid membranes and human glioblastoma cells, Bioelectrochemistry 124 (2018) 133–141, https://doi.org/10.1016/j.bioelechem.2018.07.010.
[4] L. Poltorak, M.L. Verheijden, D. Bosma, P. Jonkheijm, L.C.P.M. de Smet, E.J.R. Sudhölter, BBA - Biomembranes Lipid bilayers cushioned with polyelectrolyte-based films on doped silicon surfaces, BBA - Biomembr. 2018 (1860) 2669–2680, https://doi.org/10.1016/j.bbamem.2018.09.018.
[5] J. van Weerd, M. Karperien, P. Jonkheijm, Supported Lipid Bilayers for the Generation of Dynamic Cell-Material Interfaces, Adv. Healthc. Mater. 4 (2015) 2743–2779, https://doi.org/10.1002/adhm.201500398.
[6] Jungbae Kim, Jinwoo Lee, Hyon Bin Na, Byoung Chan Kim, Jong Kyu Youn, Ja Hun Kwak, Karam Moon, Eunwoong Lee, Jaeyun Kim, Jongnam Park, Alice Dohnalkova, Hyun Gyu Park, Man Bock Gu, Ho Nam Chang, Jay W. Grate, Taeghwan Hyeon, A Magnetically Separable, Highly Stable Enzyme System Based on Nanocomposites of Enzymes and Magnetic Nanoparticles Shipped in Hierarchically Ordered, Mesocellular, Mesoporous Silica, Small 1 (12) (2005) 1203–1207, https://doi.org/10.1002/(ISSN)1613-6829.
[7] T. Sen, I.J. Bruce, T. Mercer, Fabrication of novel hierarchically ordered porous magnetic nanocomposites for bio-catalysis, Chem. Commun. 46 (2010) 6807–6809, https://doi.org/10.1039/c0cc01747g.
[8] M. Rasmussen, S. Abdellaoui, S.D. Minteer, Enzymatic biofuel cells: 30 years of critical advancements, Biosens. Bioelectron. 76 (2016) 91–102, https://doi.org/10.1016/j.bios.2015.06.029.
[9] S.C. Barton, J. Gallaway, P. Atanassov, Enzymatic biofuel cells for implantable and microscale devices, Chem. Rev. 104 (2004) 4867–4886, https://doi.org/10.1021/cr020719k.
[10] F. Reymond, D. Fermin, H.J. Lee, H.H. Girault, Electrochemistry at liquid/liquid interfaces: methodology and potential applications, Electochim. Acta. 45 (2000) 2647–2662. http://linkinghub.elsevier.com/retrieve/pii/S0013468600003431.
[11] P. Peljo, H.H. Girault, Liquid/Liquid Interfaces, Electrochemistry at, Encycl. Anal. Chem. (2012) 1–28, https://doi.org/10.1002/9780470027318.a5306.pub2.
[12] L. Poltorak, A. Gamero-Quijano, G. Herzog, A. Walcarius, Decorating soft electrified interfaces: from molecular assemblies to nano-objects, Appl. Mater. Today. 9 (2017) 533–550, https://doi.org/10.1016/j.apmt.2017.10.001.
[13] G. Herzog, S. Flynn, C. Johnson, D.W.M. Arrigan, Electroanalytical behavior of Poly-L-lysine dendrigrafts at the interface between two immiscible electrolyte solutions, Anal. Chem. 84 (2012) 5693–5699.
[14] A. Berduque, M.D. Scanlon, C.J. Collins, D.W.M.M. Arrigan, Electrochemistry of non-redox-active poly(propylenimine) and poly(amidoamine) dendrimers at liquid-liquid interfaces, Langmuir 23 (2007) 7356–7364, https://doi.org/10.1021/la063294w.
[15] B. Devarakonda, R.A. Hill, M.M. de Villiers, The effect of PAMAM dendrimer generation size and surface functional group on the aqueous solubility of nifedipine, Int. J. Pharm. 284 (2004) 133–140, https://doi.org/10.1016/j.ijpharm.2004.07.006.

[16] M.A. González-Fuentes, J. Manríquez, R. Antaño-López, L.A. Godínez, Electrochemically driven transfer of carboxyl-terminated PAMAM dendrimers at the water/dichloroethane interface, Electrochem. Commun. 12 (2010) 137–139, https://doi.org/10.1016/j.elecom.2009.11.007.
[17] S. Ulmeanu, H.J. Lee, H.H. Girault, Voltammetric characterisation of polyelectrolyte adsorption/transfer at the water/1,2-DCE interface, Electrochem. Commun. 3 (2001) 539–543, https://doi.org/10.1016/S1388-2481(01)00209-0.
[18] C.I. Cámara, M.V.C. Quiroga, N. Wilke, A. Jimenez-Kairuz, L.M. Yudi, Effect of chitosan on distearoylphosphatidylglycerol films at air/water and liquid/liquid interfaces, Electochim. Acta. 94 (2013) 124–133, https://doi.org/10.1016/j.electacta.2013.01.137.
[19] A. Trojánek, J. Langmaier, E. Samcová, Z. Samec, Counterion binding to protamine polyion at a polarised liquid–liquid interface, J. Electroanal. Chem. 603 (2007) 235–242, https://doi.org/10.1016/j.jelechem.2007.02.006.
[20] S. Amemiya, Y. Kim, R. Ishimatsu, B. Kabagambe, Electrochemical heparin sensing at liquid/liquid interfaces and polymeric membranes, Anal. Bioanal. Chem. 399 (2011) 571–579, https://doi.org/10.1007/s00216-010-4056-2.
[21] H. Sakae, Y. Toda, T. Yokoyama, Electrochemical behavior of ferritin at the polarized water|1,2-dichloroethane interface, Electrochem. Commun. 90 (2018) 83–86, https://doi.org/10.1016/j.elecom.2018.04.010.
[22] E. Alvarez de Eulate, L. Serls, D.W.M. Arrigan, Detection of haemoglobin using an adsorption approach at a liquid-liquid microinterface array, Anal. Bioanal. Chem. 405 (2013) 3801–3806, https://doi.org/10.1007/s00216-012-6622-2.
[23] G. Herzog, V. Kam, D.W.M. Arrigan, Electrochemical behaviour of haemoglobin at the liquid/liquid interface, Electrochim. Acta. 53 (2008) 7204–7209, https://doi.org/10.1016/j.electacta.2008.04.072.
[24] S. O'Sullivan, D.W.M. Arrigan, Electrochemical behaviour of myoglobin at an array of microscopic liquid-liquid interfaces, Electrochim. Acta. 77 (2012) 71–76, https://doi.org/10.1016/j.electacta.2012.05.070.
[25] S. O'Sullivan, E. Alvarez De Eulate, Y.H. Yuen, E. Helmerhorst, D.W.M. Arrigan, Stripping voltammetric detection of insulin at liquid-liquid microinterfaces in the presence of bovine albumin, Analyst. 138 (2013) 6192–6196, https://doi.org/10.1039/c3an01123b.
[26] E. Alvarez de Eulate, S. O'Sullivan, D.W.M. Arrigan, Electrochemically induced formation of cytochrome c oligomers at soft interfaces, ChemElectroChem. 4 (2017) 898–904, https://doi.org/10.1002/celc.201600851.
[27] B.M.B. Felisilda, D.W.M. Arrigan, Electroactivity of aptamer at soft microinterface arrays, Anal. Chem. 90 (2018) 8470–8477, https://doi.org/10.1021/acs.analchem.8b01172.
[28] J.J. Nieminen, I. Hatay, P. Ge, M.A. Méndez, L. Murtomäki, H.H. Girault, Hydrogen evolution catalyzed by electrodeposited nanoparticles at the liquid/liquid interface, Chem. Commun. 47 (2011) 5548–5550, https://doi.org/10.1039/c1cc10637f.
[29] M. Platt, R.A.W. Dryfe, E.P.L. Roberts, Structural and electrochemical characterisation of Pt and Pd nanoparticles electrodeposited at the liquid/liquid interface, Electochim. Acta. 49 (2004) 3937–3945, https://doi.org/10.1016/j.electacta.2004.02.050.
[30] P.S. Toth, A.N.J. Rodgers, A.K. Rabiu, R.A.W. Dryfe, Electrochemical activity and metal deposition using few-layer graphene and carbon nanotubes assembled at the liquid–liquid interface, Electrochem. Commun. 50 (2015) 6–10, https://doi.org/10.1016/j.elecom.2014.10.010.
[31] A. Uehara, T. Hashimoto, R.A.W. Dryfe, Au electrodeposition at the liquid-liquid interface: mechanistic aspects, Electochim. Acta 118 (2014) 26–32, https://doi.org/10.1016/j.electacta.2013.11.162.
[32] L. Poltorak, M. Hébrant, M. Afsharian, M. Etienne, G. Herzog, A. Walcarius, Local pH changes triggered by photoelectrochemistry for silica condensation at the liquid-liquid interface, Electrochim. Acta 188 (2016) 71–77, https://doi.org/10.1016/j.electacta.2015.11.107.
[33] L. Poltorak, G. Herzog, A. Walcarius, In-situ formation of mesoporous silica films controlled by ion transfer voltammetry at the polarized liquid–liquid interface, Electrochem. Commun. 37 (2013) 76–79, https://doi.org/10.1016/j.elecom.2013.10.018.
[34] S. Senthilkumar, R.A.W. Dryfe, R. Saraswathi, Size-selective voltammetry: modification of the interface between two immiscible electrolyte solutions by zeolite Y, Langmuir 23 (2007) 3455–3461.
[35] H. Jänchenová, K. Štulík, V. Mareček, Preparation of a silicate membrane at a liquid|liquid interface and its doping with a platinum ion, J. Electroanal. Chem. 591 (2006) 41–45, https://doi.org/10.1016/j.jelechem.2006.03.036.
[36] V. Mareček, H. Jänchenová, Electrochemically controlled formation of a silicate membrane at a liquid|liquid interface, J. Electroanal. Chem. 558 (2003) 119–123, https://doi.org/10.1016/S0022-0728(03)00386-3.
[37] L. Poltorak, N. van der Meijden, S. Oonk, E.J.R. Sudhölter, M. de Puit, Acid phosphatase behaviour at an electrified soft junction and its interfacial co-deposition with silica, Electrochem. Commun. 94 (2018) 27–30, https://doi.org/10.1016/j.elecom.2018.07.022.
[38] J. Niedziolka, M. Opallo, Electrochemically assisted sol–gel process at a three phase junction, Electrochem. Commun. 10 (2008) 1445–1447, https://doi.org/10.1016/j.elecom.2008.07.039.
[39] H.J. Lee, P.D. Beattie, B.J. Seddon, M.D. Osborne, H.H. Girault, Amperometric ion sensors based on laser-patterned composite polymer membranes, J. Electroanal. Chem. 440 (1997) 73–82, https://doi.org/10.1016/S0022-0728(97)80042-3.
[40] Z. Samec, Electrochemistry at the interface between two immiscible electrolyte solutions (IUPAC technical report), Pure Appl. Chem. 76 (2004) 2147–2180.
[41] X. Jiang, K. Gao, D. Hu, H. Wang, S. Bian, Y. Chen, Ion-transfer voltammetric determination of folic acid at meso-liquid–liquid interface arrays, Analyst. 140 (2015) 2823–2833, https://doi.org/10.1039/C4AN02011A.
[42] L. Xie, X. Huang, X. Lin, B. Su, Nanoscopic liquid/liquid interface arrays supported by silica isoporous membranes: Trans-membrane resistance and ion transfer reactions, J. Electroanal. Chem. 784 (2017) 62–68, https://doi.org/10.1016/j.jelechem.2016.12.007.
[43] L. Xie, X. Huang, B. Su, Portable sensor for the detection of choline and its derivatives based on silica isoporous membrane and gellified nanointerfaces, ACS Sensors 2 (2017) 803–809, https://doi.org/10.1021/acssensors.7b00166.
[44] Y. Chen, S. Bian, K. Gao, Y. Cao, H. Wu, C. Liu, X. Jiang, X. Sun, Studies on the meso-sized selectivity of a novel organic/inorganic hybrid mesoporous silica membrane, J. Memb. Sci. 457 (2014) 9–18, https://doi.org/10.1016/j.memsci.2014.01.035.
[45] Partition Coefficient Calculation with ACD/LogP, (n.d.). (accessed January 14, 2020). https://www.acdlabs.com/products/percepta/predictors/logp/.
[46] D.R. Lide, CRC Handbook of Chemistry and Physics, 84th Edition, 2003-2004, Handb. Chem. Phys. 53 (2003) 2616.
[47] E.R. Lippincott, A. Vanvalkenburg, C.E. Weir, E.N. Bunting, Infrared studies on polymorphs of silicon dioxide and germanium dioxide, J. Res. Natl. Bur. Stand. 61 (1958) (1934) 61, https://doi.org/10.6028/jres.061.009.
[48] P.J. Launer, B. Arkles, Infrared Analysis of Orgaonsilicon Compounds, in: Silicon Compd. Silanes Silicones (3rd Ed.), 2013: pp. 175–178.
[49] G. Herzog, W. Moujahid, J. Strutwolf, D.W.M. Arrigan, Interactions of proteins with small ionised molecules: electrochemical adsorption and facilitated ion transfer voltammetry of haemoglobin at the liquid/liquid interface, Analyst. 134 (2009) 1608–1613, https://doi.org/10.1039/b905441n.
[50] G. Herzog, P. Eichelmann-Daly, D.W.M. Arrigan, Electrochemical behaviour of denatured haemoglobin at the liquid|liquid interface, Electrochem. Commun. 12 (2010) 335–337, https://doi.org/10.1016/j.elecom.2009.12.020.
[51] D.W.M. Arrigan, G. Herzog, M.D. Scanlon, J. Strutwolf, Bioanalytical applications of electrochemistry at liquid-liquid microinterfaces, Electroanal. Chem. A Ser. Adv. 25 (2013) 105–178.
[52] D.W.M. Arrigan, M.J. Hackett, R.L. Mancera, Electrochemistry of proteins at the interface between two immiscible electrolyte solutions, Curr. Opin. Electrochem. 12 (2018) 27–32, https://doi.org/10.1016/j.coelec.2018.07.012.
[53] C. Chaiyasut, Y. Takatsu, S. Kitagawa, T. Tsuda, Estimation of the dissociation constants for functional groups on modified and unmodified silica gel supports from the relationship between electroosmotic flow velocity and pH, Electrophoresis 22 (2001) 1267–1272, https://doi.org/10.1002/1522-2683(200105)22:7<1267::AID-ELPS1267>3.0.CO;2-8.
[54] L.K. Tamm, S. Tatulian, Infrared spectroscopy of proteins and peptides in lipid bilayers infrared spectroscopy of proteins and peptides in lipid bilayers, Quaterly Rev. Biophys. 4 (1997) 365–429, https://doi.org/10.1017/S0033583597003375.